Magnetic Nanoparticles for Radio Frequency Hyperthermia: Preparation and Surface Functionalization Effects on Cellular Uptake

Stanley E. Gilliland III[1,2], Everett E. Carpenter[2], and Michael D. Shultz[1,2,*]

[1]Research and Development, Hunter Holmes McGuire VA Medical Center, Richmond, VA 23249,
gillilandse@vcu.edu, ecarpenter2@vcu.edu
[2]Department of Chemistry,
Virginia Commonwealth University, Richmond, VA 23284,
*shultzmd@vcu.edu

ABSTRACT

Iron oxide nanoparticles have received sustained interest for biomedical applications such as radio frequency hyperthermia. The principles of LaMer growth, mixed diffusion-reaction growth, and Ostwald ripening were used to tune the crystallite size and size distribution of iron oxide nanoparticles for maximum radio frequency heating. Radio frequency heating rates of up to 5.55 (°C/min)/mg (ILP = 3.11 nHm^2/kg, H = 37.4 kA/m and f = 270 kHz) were achieved by the benzyl alcohol modified seed growth of iron oxide nanoparticles. Additionally, the iron oxide nanoparticles are easily and rapidly surface functionalized with (3-aminopropyl) trimethoxysilane, (3-aminopropyl) triethoxysilane or carboxymethylated polyvinylalcohol. Initial *in vitro* uptake experiments were used to investigate differences based on zeta potential.

Keywords: iron oxide nanoparticle, cell uptake, surface functionalization, LaMer growth, Ostwald ripening

1 INTRODUCTION

In 1957 Gilchrist first reported the idea of using magnetic particles for hyperthermia treatment of tumors [1]. The extent and rate of particle heating depends on the size, conductivity and magnetic properties of the material [1]. More specifically, iron oxide nanoparticles (NPs) are a primary candidate for nanomedicine therapeutic applications due in part to their radio frequency (RF) induction heating properties, as well as being biocompatible and biodegradable [2,3]. In addition, they can be classified as a theranostic agent [4] providing diagnostic imaging capabilities in the form of a MRI contrast [5] and therapeutic potential by means of Magnetic Fluid Hyperthermia (MFH) [3,5].

Superparamagnetic iron oxide NPs generate heat by the Néel and Brownian relaxation mechanisms [2]. The Néel heating mechanism dominates at small particle sizes and Brownian mechanism takes over at larger particle sizes [2,6]. The optimal iron oxide NPs for heat generation by RF induction heating have been reported to have a crystallite size of 15-16 nanometers (nm) [6]. The main challenge to overcome is to develop an iron oxide synthesis that produces iron oxide NPs that are easily surface functionalized for biostability and targeting for increased tumor uptake [2]. Thus, optimization and investigation of iron oxide NP synthesis to control and obtain the best combination of properties, while maintaining minimal toxicity and ease of surface functionalization is of growing interest in radio frequency hyperthermia applications.

Herein, the principles LaMer growth, mixed diffusion-reaction growth, and Ostwald ripening are used to tune the size distribution and crystallite size of iron oxide NPs. The synthesis using benzyl alcohol as the solvent, capping agent and reducing agent for the combined reduction and thermal decomposition of iron (III) acetylacetonate ($Fe(acac)_3$) offers the benefits of a simplistic synthesis and ease of surface functionalization [7]. The NPs are then surface functionalized with (3-aminopropyl) trimethoxysilane (APTS), (3-aminopropyl) triethoxysilane (APTES) or carboxymethyl polyvinyl alcohol (CMPVA) to demonstrate the ease of surface functionalizing benzyl alcohol synthesized NPs, and to initially investigate cell uptake based on different surface charges.

2 MATERIALS AND METHODS

Iron oxide NPs were synthesized by procedures as previously reported [7]. In investigating the mechanism of synthetic control, these studies manipulated reaction amounts and temperatures according to the following naming system. A and B denote the first or second additions of $Fe(acac)_3$ respectively and are separated by an underscore. The A and B are followed by numbers indicating the gram amount of $Fe(acac)_3$ added at the respective addition. This is followed by a "-X" with X indicating the time in hours the reaction proceeded before a subsequent addition. When temperature was investigated as a parameter, it is indicated by the number in parenthesis beside the reaction time. A2-24(175)_B2-24(175) for example indicates a reaction with 2 g of $Fe(acac)_3$ initially added to 20 mL of benzyl alcohol in the presence of air. This was reacted for 24 hours at 175°C before a second addition of $Fe(acac)_3$, which was then reacted for 24 hours at 175°C. Each reaction was characterized using XRD, VSM corrected by TGA, RF heating corrected by Prussian blue analysis, and DLS to determine crystallite size,

Table 1. Nanoparticle characterization of reactions with varying precursor concentrations. Saturation Magnetization, Heating Profile, and Average Size determined by VSM, Heating Induction, XRD, and DLS.

Reaction	Magnetization (emu/g)	RF Heating ([ºC/min]/mg)	Crystallite size (nm)	Hydrodynamic Diameter (nm)	PDI
A2-24(205)	73.36	2.76	14.1 ± 0.80	24.53	0.275
A4-24(205)	73.07	1.86	11.7 ± 0.73	22.85	0.269
A6-24(205)	69.93	0.85	8.2 ± 1.56	23.9	0.512
A2-24(195)_B2-24(195)	78.202	4.04	14.9 ± 0.74	37.52	0.219
A2-24(205)_B2-24(205)	79.35	5.55	19.5 ± 1.06	44.63	0.265
A4-24(195)_B2-24(195)	75.12	3.13	14.95 ± 2.03	29.5	0.36
A4-24(195)_B4-24(195)	76.56	4.48	13.4 ±1.61	31.94	0.121
A4-24(195)_B6-24(195)	76.99	3.43	15.2 ± 1.50	26.6	0.112
A4-24(205)_B6-24(205)	85.26	3.14	15.3 ± 2.45	28.2	0.14
A6-24(195)_B2-24(195)	71.64	2.71	11.4 ± 1.25	43.89	0.305
A6-24(195)_B4-24(195)	72.74	2.88	12.9 ± 0.92	23.5	0.176
A6-24(195)_B6-24(195)	75.1	2.58	14.1 ±0.98	26.19	0.231

magnetization saturation (M_S), RF heating, and hydrodynamic diameter, PDI, and zeta potential values respectively. Iron oxide NPs were surface functionalized with CMPVA as done previously [7]. Surface functionalization with APTS or APTES was carried out with modifications to methods in the literature [7]. Briefly, 10 mg of iron oxide NPs were dissolved in 0.125% TMAOH solution by sonication for 30 minutes. Next, 8 mL of water was added and then 0.0102 mol of either APTS or APTES was added dropwise while heating and stirring at 60℃ for 1 hour. The pH was adjusted to about 7.4 and then buffer exchanged in a 30k molecular weight cutoff centrifugal filter and washed 3 times with 15 mL of water. The resulting solution was then sterile filtered with a 0.2 µm filter.

GBM6 cells (provided by Dr. C. David James – University of California, San Fransico, Department of Neurological Surgery) were cultured under conditions for other cell types as reported [7]. For cell uptake experiments, cells were harvested and plated (150,000 cells in 2 mL of medium per well) in 6 well plates and incubated overnight. Cells were treated with either 200 µL of cell medium or CMPVA, APTS, or APTES coated iron oxide NPs (0.2 µm sterile filtered, 250 µg/mL) in triplicate. After 4 hours of incubation, cells were rinsed with PBS three times, collected by scraping with a cell lifter in 1 mL of PBS and pelleted by centrifugation. Then 30 µL of cell lysis buffer (CellLytic M) was added to the cell pellet and sonicated for 15 minutes before 2.14 µL of 70% nitric acid was added. The cell suspension was heated at 95℃ to completely lyse the cells and dissolve the iron oxide NPs. Prussian blue analysis was performed by adding 10 µL of sample to 1 µL of 20% Prussian blue and 0.5 µL of 20% of hydrochloric acid and incubating at room temperature for 15 minutes before collecting UV-Vis absorption (λ=685 nm). A standard curve was produced by Prussian Blue UV-Vis absorption assay (λ=685 nm) with a Fe ICP standard (Alfa Aesar) and UV-Vis absorption with a Nanoquant plate reader (Tecan).

3 RESULTS AND DISCUSSION

Based on the previous results [7] and principles of LaMer growth model, it was thought that the crystallite size and polydispersity could be further controlled by increasing the temperature to 205℃ and varying the concentration of iron precursor. The LaMer growth model, **Figure 1 (solid blue curve)**, illustrates how nanoparticles are formed from a precursor solution. The model first indicates the formation of monomers, followed by self-nucleation and growth processes [8]. Once the solubility concentration is reached, Ostwald ripening will occur to lower the surface energy of NPs by dissolving the smaller NPs that will then grow on larger NPs [9]. In **Table 1**, increasing the $Fe(acac)_3$ amount by 2 grams per reaction, (A2-24, A4-24 and A6-24) resulted in no significant change in crystallite size, but showed an increase in the hydrodynamic diameter and decrease in polydispersity index (PDI) (note: lower PDI corresponds to a more monodisperse solution). The increase in overall particle size and decrease in PDI is in accordance with the principles of the LaMer growth model [8].

Interestingly, increasing the concentration of $Fe(acac)_3$ led to a decrease of crystallite size when the reaction temperature was increased to 205°C (**Table 1**). Although the crystallite size decreased, the hydrodynamic diameters remained constant while the PDI increased at the highest concentration of $Fe(acac)_3$ (6 g). Increasing the temperature will add energy in to the system so that generation of monomers, rate of nucleation, and diffusion/reaction rates of growth will all increase (depicted in **Figure 1)**. The increase of the polydispersity in reaction A6-24(205) can potentially be explained with the theory of mixed diffusion-reaction growth [10]. Growth is controlled depending on whether growth by diffusion or growth by reaction is the rate limiting step [10]. In the case of A6-24(205) the concentration of Fe is so high that diffusion is very quick and therefore growth is controlled by how fast the Fe can react with the surface of nuclei leading to larger size distributions[10].

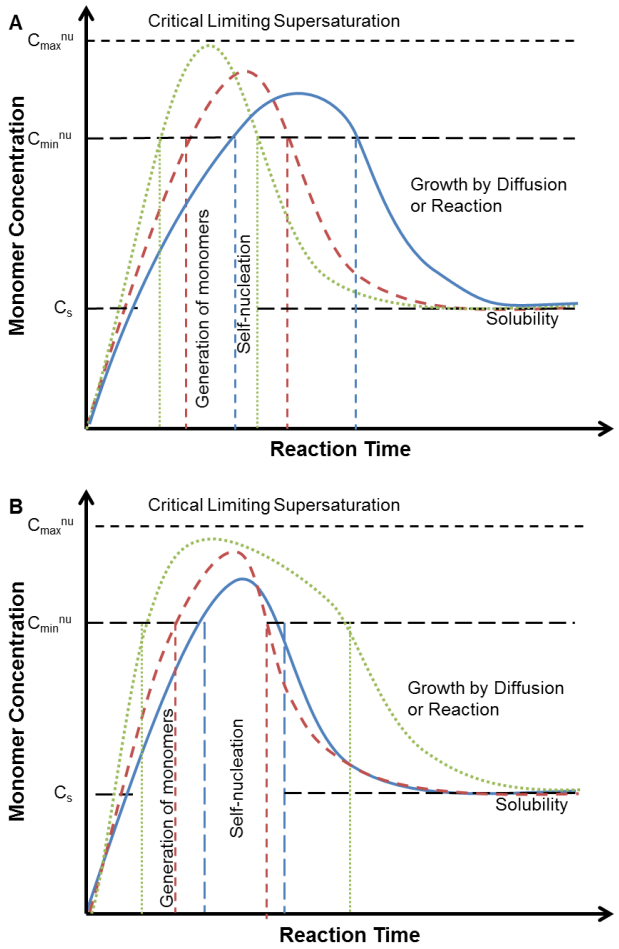

Figure 1. Schematic representation of LaMer growth model (solid blue) and theorized effects of concentration and temperature on the generation of monomers, formation of nuclei, and growth by diffusion or reaction. C_S, C_{min}^{nu}, and C_{max}^{nu} are the concentration that are stable in solution, the concentration at which nucleation begins, and the concentration where the rate of nucleation becomes infinite, respectively.

Additionally, it is thought that the rate of particle growth will be faster than crystalline growth which explains the smaller crystallite size with the same hydrodynamic size, as seen for the reactions A2-24(205), A4-24(205), and A6-24(205). For reactions A2-24(205) and A4-24(205), growth is thought to be limited by diffusion which gives rise to smaller PDI values. Also, in corroboration, at lower concentrations the rate of diffusion will be even slower allowing for more crystalline growth rather than amorphous growth. More specifically, this can be further rationalized using the LaMer growth models in **Figure 1 A and B**. The first rationale (**Figure 1A**.), is explained by both temperature and concentration increasing the rate of monomer production leading to higher rates of nucleation. The second rationale (**Figure 1B)** uses this same effect of temperature and concentration; however, it is thought that sufficiently high precursor concentrations and elevated temperatures will prolong the nucleation stage. The shifting of peaks to earlier time points in **Figure 1A** corresponds with an increased rate of monomer production to reach the higher concentrations of monomers at earlier time points. Thus with an increased rate of monomer production it is thought that a higher nucleation rate will be reached causing a quicker "burst" nucleation event leading to the same number of nuclei formed, but with growth limited by reaction rather than diffusion. Due to this it is believed that at some increased concentration the monomers will have less time to grow in a crystalline manner and will grow amorphously.

An alternative reasoning for the trend of decreasing crystallite sizes is thought to be due to a prolonged nucleation stage as well as higher rates of nucleation reached (**Figure 1B**). The LaMer growth model suggests that in order for the nucleation stage to end and growth stage to begin, the monomer concentration must drop below the critical supersaturation limit (C_{min}^{nu}) [8,10]. In these reactions, the higher temperature and concentration of $Fe(acac)_3$ produces monomers faster than they can self-nucleate to deplete the concentration of monomers below the C_{min}^{nu} (**Figure 1B**, dotted green and dashed red curves). This leads to a higher peak where nucleation rates are faster causing more monodisperse nuclei to form before the reaction switches completely to growth. For reaction A4-24(205), this produces more nuclei that are smaller in size. At this concentration, the growth is switching from limited by diffusion to limited by reaction. This will lead to growth that is more amorphous than crystalline, but with similar PDI and hydrodynamic values as compared to A2-24(205). When the concentration of iron precursor is further increased, A6-24(205), the peak concentration of monomers is further elevated. At this concentration, a threshold is crossed and the limit of production of monomers may have been reached. Production of monomer then will continue to occur even at high rates of nucleation leading to an extended nucleation event (**Figure 1B** dotted green curve). Additionally, the rate of diffusion is much faster than the rate of reaction leading to even more amorphous growth compared to amount of crystallite growth.

The increase in PDI for reaction A6-24(205) may be explained from two perspectives. First, in **Figure 1A**, when Ostwald ripening begins, the lower concentration reactions are polydisperse which leads to a monodisperse system. In contrast, the higher concentrations which are monodisperse at the beginning of Ostwald ripening will lead to a polydisperse system and thus increased PDI. Second, in **Figure 1B**, the high concentration reaction and prolonged nucleation stage prevented sufficient time for Ostwald ripening to lower the PDI. However, the concentration increase from A2-24(205) to A4-24(205) may not be large enough to drastically change the PDI.

Next, a series of modified seed growth syntheses were conducted in an attempt to further tune the crystallite size and PDI to obtain maximum RF heating rates. The modified seed growth conditions are shown in **Table 1**. The reaction

A2-24(205)_B2-24(205) yielded the highest crystallite and hydrodynamic diameter with a relatively low PDI value, and had the highest RF heating value of all reactions investigated. While the principles of LaMer growth, mixed diffusion-reaction growth, and Ostwald ripening principles are harder to discern in the modified seed growth methods, they are invaluable in fine tuning the crystallite size and PDI to obtain high RF heating rates.

Modifying the surface of iron oxide NPs is essential for biostability and further conjugation. CMPVA can be attached to the surface of iron oxide through strong interactions with the carboxyl groups [7,11]. APTS and APTES form a silane shell around iron oxide NPs and can directly bond to OH groups on the surface [12]. Successful functionalization was confirmed by obtaining a stable solution of particles and by FTIR analysis. CMPVA iron oxide NPs were previously optimized and confirmed using FTIR [7]. The APTS and APTES iron oxide NPs were surface functionalized with equal molar ratio of APTS and APTES. The FTIR data showed an appearance of peaks at 1030 and 1305 cm^{-1} indicating Si-O-Si and C-N stretching vibrations respectively [12].

Initial cellular uptake studies were conducted to compare iron oxide NPs surface functionalized with either cationic groups (APTS and APTES) or anionic groups (CMPVA) thereby altering their effective surface charge. The zeta potentials measured were -19.2±0.94 for CMPVA, 21.5±1.33 for APTS, and 21.1±1.94 for APTES. In aggrement with other reports, the positively charged APTS and APTES NPs had a higher amount of iron per cell compared to the negatively charged CMPVA (**Figure 2**). Interestingly, the CMPVA NPs were stable in water for several months, while the APTS and APTES NPs were only stable in water for a few days. The stability in different biologically relevant media could potentially shed light on differences in cellular uptake/association.

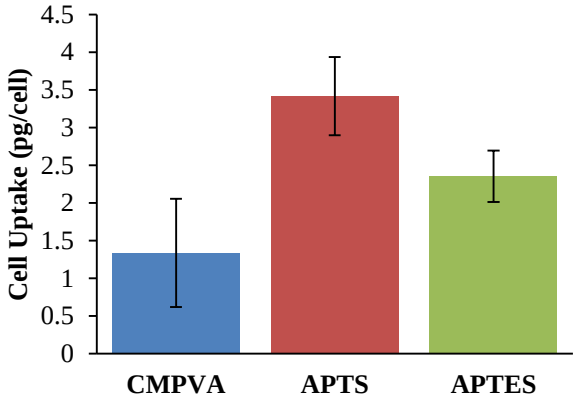

Figure 2. Cell uptake measurements in units of picograms per cell.

4 CONCLUSION

The modified seed growth of iron oxide nanoparticles in benzyl alcohol has been shown to follow principles of LaMer growth, mixed diffusion growth, and Ostwald ripening, thus providing the ability to tune the nanoparticles crystallite size and size distribution for increased radio frequency induced magnetic heating applications. Further studies are needed to completely elucidate the effects of elevated temperature and increased precursor concentrations, as there are two possible explanations for these effects on crystallite size and size distribution. The initial *in vitro* uptake experiments showed that positive zeta potential nanoparticles had higher cell uptake. However, future studies may reveal that colloidal stability could artificially augment uptake results thus prompting the need for more thorough investigation.

5 ACKNOWLEDGEMENTS

Research support was provided by the Department of Veterans Affairs, Veterans Health Administration, Office of Research and Development, Biomedical Laboratory Research and Development through a Career Development Award grant 1IK2BX001561-01A2 to MD Shultz. The contents of this article do not represent the views of the Department of Veterans Affairs or the United States Government.

6 REFERENCES

[1] Gilchrist, R. K.; Medal, R.; Shorey, W. D.; Hanselman, R. C.; Parrott, J. C.; Taylor, C. B. *Ann. Surg*, 146, 1957.

[2] Torres-Lugo, M.; Rinaldi, C. *Nanomedicine*, 8, 1689-1707, 2013.

[3] Hergt, R.; Dutz, S.; Mueller, R.; Zeisberger, M. *Journal of Physics-Condensed Matter,18*, S2919-S2934, 2006.

[4] Wilson, J. D.; Broaddus, W. C.; Dorn, H. C.; Fatouros, P. P.; Chalfant, C. E.; Shultz, M. D. *Bioconjug. Chem.*, *23*, 1873-1880, 2012.

[5] Gupta, A.; Gupta, M. *Biomaterials*, *26*, 3995-4021, 2005.

[6] Deatsch, A. E.; Evans, B. A. *J Magn Magn Mater*, *354*, 163-172, 2014.

[7] Gilliland III S, Carpenter E, Shultz M. *Nanobiomedicine*, 1:9. doi: 10.5772/60035; 2014.

[8] LaMer, V. K.; Dinegar, R. H. *J. Am. Chem. Soc.*, *72*, 4847-4854, 1950.

[9] Murray, C.; Norris, D.; Bawendi, M. *J. Am. Chem. Soc.*, *115*, 8706-8715, 1993.

[10] Rao, C. N. R.; Müller, A.; Cheetham, A. K. *Nanomaterials chemistry : recent developments and new directions;* Weinheim : Wiley-VCH ; Chichester : John Wiley, distributor: Weinheim : Chichester, 2007 .

[11] Johannsen, M.; Gneveckow, U.; Taymoorian, K.; Thiesen, B.; Waldoefner, N.; Scholz, R.; Jung, K.; Jordan, A.; Wust, P.; Loening, S. A. *International Journal of Hyperthermia*, *23*, 315-323, 2007.

[12] Mohapatra,S.; Pramanik,N.; Mukherjee,S.; Ghosh,S. K..; Pramanik,P. *J. Mater. Sci.*, 42, 7566-7574, 2007.